Thermal step bunching and interstep attraction on the vicinal surface with adsorption

Noriko Akutsu
Faculty of Engineering, Osaka Electro-Communication University, Hatsu-cho, Neyagawa, Osaka 572-8530, Japan

Yasuhiro Akutsu
Department of Physics, Graduate School of Science, Osaka University, Machikaneyama-cho, Toyonaka, Osaka 560-0043, Japan

Takao Yamamoto
Department of Physics, Faculty of Engineering, Gunma University, Kiryu, Gunma 376-0052, Japan
(Received 28 September 2002; published 12 March 2003)

We study statistical thermodynamical behavior of the vicinal surface with adsorption. We consider the case where attractive lateral interactions between adsorbates are present, which cause the thermal step bunching. As the microscopic model Hamiltonian for the vicinal surface with adsorption, we adopt a restricted-solid-on-solid model coupled with the Ising system. Using the density-matrix renormalization group algorithm, we obtain surface-free energy and adsorption coverage as functions of the surface slope p. We derive the step tension and the step-interaction coefficient from the free energy. We clarify the origin of the thermal step bunching and the adsorbate-mediated interstep attraction.

DOI: 10.1103/PhysRevB.67.125407 PACS number(s): 68.35.Md, 68.43.−h, 05.70.Np, 05.50.+q

I. INTRODUCTION

For the surface with adsorbates, there are numbers of experimental or theoretical studies on the equilibrium surface structure with adsorbates.[1–4] The surface is often reconstructed by adsorbates; the superlattice is formed due to the excluded volume effect of the adsorbates and the elastic interactions among adsorbates and the substrate.

From the viewpoint of the crystal growth, the ''excited'' structures on the surface such as the surface steps, kinks in a step, and ad islands/negative islands are important, since the microscopic crystal growth occurs on such places. The vicinal (tilted) surface is especially important from the same point of view;[4–7] the steps on the vicinal surface play the role of the ''linear sink'' of the adatoms on the surface. When the adsorbates exist on the surface, we should study the interplay between adsorbates and the excited structures, since the interplay may cause nontrivial effects on the behavior of the system.

Nevertheless, the theoretical study on the interplay between the excited structures on the surface and adsorbates has not been done sufficiently yet. One reason is the difficulty to construct effective models to explain the experimental results; the vicinal surface with adsorbates shows wide variety of phenomena depending on temperature, adsorption vapor pressure, and the combination of materials. Another reason is the difficulty to make the precise estimation of the ''entropic effect.'' The vicinal surface belongs to the Gruber-Mullins-Pokrovsky-Talapov (GMPT) universality class and is in the ''critical'' state.[8–16] Reliable calculation of thermodynamic quantities in such a critical state is extremely difficult, in general.

Recently, a highly reliable numerical algorithm called the density-matrix renormalization group (DMRG) has been devised.[17] The DMRG, which is originally applied to quantum spin chains, have been successfully applied to two-dimensional (2D) statistical-mechanical problems.[18] What we will use in the present work is a variation of the DMRG, called the product wave-function renormalization group[19] (PWFRG) which is suitable for study of vicinal-surface-type critical state.[20–22]

The simplest case of the zero-lateral interaction between adsorbates (Langmuir adsorption[1]) has been studied in our previous paper.[23] We presented a decorated restricted-solid-on-solid (RSOS) model, and made detailed statistical-mechanical study on the roughening transition temperature T_R, surface-free energy, adsorption coverage Θ, step tension γ, and step stiffness $\tilde{\gamma}$. We showed that the decorated RSOS model is exactly mapped to the original RSOS model with the effective microscopic ledge energy ϵ^{eff}. The decorated RSOS model shows the GMPT universal behavior.[8–16] From the exact analytic equation of ϵ^{eff}, we pointed out the occurrence of the multireentrant roughening transition.

For the case of nonzero-lateral interaction between adsorbates, we presented the RSOS model coupled with the Ising system (RSOS-I model) in Refs. 24,25. We found that the first-order transition occurs on the equilibrium crystal shape (ECS), below the roughening transition temperature; this transition accompanies *the thermal step bunching* or *the quasifacet formation*[24,25] (see Fig. 1). We also found that interstep attraction seems to emerge upon adsorption.[25]

The aim of the present paper is to clarify the origin of the thermal step bunching and the interstep attraction. For this purpose, we investigate the RSOS-I model in detail; in particular, from the microscopic RSOS-I model Hamiltonian, we obtain the explicit functional form of the surface-free energy near the first-order transition. We also give surface slope dependence of the adsorption coverage.

This paper is organized as follows. In Sec. II, we explain the RSOS-I model Hamiltonian of the vicinal surface with adsorption. In Sec. III, we give brief explanation of the calculation method for surface quantities. In Sec. IV, we consider the case where the steps are weakly coupled with adsorbates (''physisorption'' case). We give results of the

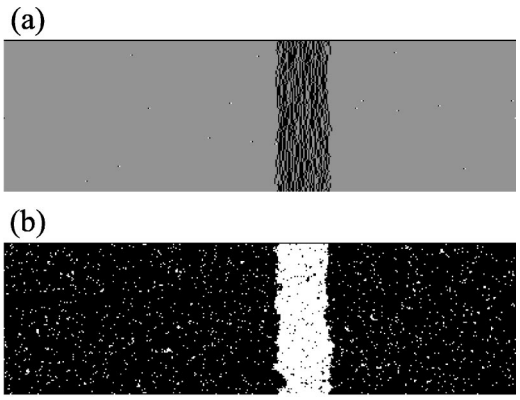

FIG. 1. An example of the adsorption-induced thermal step bunching in the RSOS-I model (Sec. II; top view of the surface of size 408×120 and with 24 steps on it): A snapshot of the Monte Carlo simulation at 1×10^7 MCS for $\alpha=0.1$, $J/\epsilon=0.25$, $H/\epsilon=(\mu/2+J)/\epsilon=-0.02$, and $k_BT/\epsilon=0.5$. (a) The step condensation: The configuration of the RSOS vicinal surface is shown, where a white (black) point indicates $h(m+1,n)-h(m,n)=\Delta_x(m,n)=1$ (-1). (b) The adsorbate segregation: The configuration in the adsorption layer (Ising system) is shown, where white dots represent adsorbates (up spins). The RSOS system of (a) is covered with the adsorption system of (b).

PWFRG calculation. We explain the relationship between the first-order transition on the ECS and the thermal step bunching (or the quasifacet formation). The step-tension γ and the step interaction coefficient g are shown. In Sec. V, we explain how the interchange between the ordered states cause the first-order transition on the ECS, based on the form of the free energy obtained by the PWFRG. In Sec. VI, we consider the case where the steps are strongly coupled with adsorbates (''chemisorption'' case). We show that the first-order transition occurs without the interchange between the ordered states. In Sec. VII, we show how the adsorbate-mediated interstep attraction is generated. Calculated results of γ and g for the strong-coupling case is given in the section. To understand the dip in the temperature dependence of g, we give an explanation based on the step-droplet picture. In Sec. VIII, we mention the application to real systems. In Sec. IX, we give summary of the paper.

II. SURFACE MODEL WITH ADSORPTION

A. RSOS-Ising coupled model

In order to treat steps, islands, and negative islands on a crystal surface, we consider an SOS model on a square lattice with nearest-neighbor (nn) interactions. The position of each SOS column is expressed in terms of a pair of integers as (m,n). The height of the column is denoted by $h(m,n)$ [Fig. 2(a)].

For simplicity, we impose the RSOS condition[26,27] such that the nn height difference Δh should be $\Delta h=0,\pm1$. This simplification is reasonable, because configurations with large $|\Delta h|$ are energetically unfavorable. The Hamiltonian of the RSOS system is written as follows:

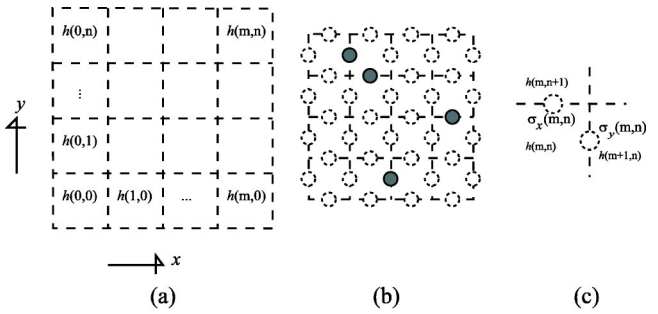

FIG. 2. (a) The top view of the RSOS model. The column height $h(m,n)$ is assigned on the 2D square lattice with the site of (m,n). The height difference between nn sites Δh is restricted to $\{1,0,-1\}$. (b) 2D square lattice-gas (Ising) model, where the filled circle represents the adsorbate (the up spin), and the open circle with dashed line denotes empty site (the down spin). (c) Adsorption sites on the RSOS surface.

$$\mathcal{H}_{\mathrm{RSOS}}=\sum_{m,n}\left[\epsilon|h(m+1,n)-h(m,n)|+\epsilon|h(m,n+1)-h(m,n)|\right], \tag{2.1}$$

where ϵ is the microscopic ledge energy, and the summation with respect to (m,n) is taken over all sites of the lattice points. The RSOS condition is taken into account implicitly. The statistical-mechanical behavior of the RSOS model is well known,[26,27] and the roughening transition temperature T_R of the RSOS model[27] is given by

$$\frac{\epsilon}{k_BT_R}=0.633. \tag{2.2}$$

In order to describe configurations of the monolayer adsorbate system, we consider 2D nn Ising model, where each value of the Ising spin ±1 corresponds to presence/absence of the adsorbates. The adsorbate is assumed to be put on the bridge site of the RSOS surface [Fig. 2(b)]. We denote the Ising spin at the side between $h(m,n)$ and $h(m+1,n)$ as $\sigma_y(m,n)$, and at the side between $h(m,n)$ and $h(m,n+1)$ as $\sigma_x(m,n)$ [Fig. 2(c)].

The Hamiltonian of the adsorbates system is written as follows:

$$\mathcal{H}_{\mathrm{Ising}}=-J\sum_{m,n}\left[\sigma_x(m,n)\sigma_y(m,n)+\sigma_x(m,n)\sigma_y(m-1,n)+\sigma_x(m,n-1)\sigma_y(m,n)+\sigma_x(m,n-1)\sigma_y(m-1,n)\right]-H\sum_{m,n}\left[\sigma_x(m,n)+\sigma_y(m,n)\right], \tag{2.3}$$

where J is the coupling constant (for lateral interaction among adsorbates), and H is the external field (surface chemical potential). The Ising system also forms a square lattice, which is 45° rotated from the RSOS lattice. The statistical-mechanical behavior of the 2D Ising system is well known,[1,5,28,29] and the order-disorder transition temperature T_c is exactly known as

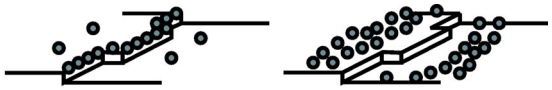

FIG. 3. Schematic figure for the relation between the step ledge and the adsorbates. When $\alpha=0$, the surface system is independent of the adsorption system.

$$\frac{J}{k_B T_c}=\frac{1}{2}\ln(1+\sqrt{2}). \tag{2.4}$$

As a microscopic effect of the adsorbates to the surface atoms, we introduce a microscopic coupling constant α such that ϵ is replaced by $\epsilon(1-\alpha\sigma)$. When $\alpha>0$, an adsorbate favors the ledge site, and when $\alpha<0$, the adsorbate avoids the ledge site (Fig. 3).

The total Hamiltonian for the RSOS-I model is written as follows:

$$\begin{aligned}\mathcal{H}_{\mathrm{RSOS-I}}&=\mathcal{H}_{\mathrm{RSOS}}+\mathcal{H}_{\mathrm{Ising}}+\mathcal{H}_{\mathrm{int}}\\&=\sum_{m,n}\left[\epsilon\{1-\alpha\sigma_y(m,n)\}|h(m+1,n)-h(m,n)|\right.\\&\quad\left.+\epsilon\{1-\alpha\sigma_x(m,n)\}|h(m,n+1)-h(m,n)|\right]\\&\quad-J\sum_{m,n}\left[\sigma_x(m,n)\sigma_y(m,n)+\sigma_x(m,n)\sigma_y(m-1,n)\right.\\&\quad+\sigma_x(m,n-1)\sigma_y(m,n)+\sigma_x(m,n-1)\sigma_y\\&\quad\left.\times(m-1,n)\right]-H\sum_{m,n}\left[\sigma_x(m,n)+\sigma_y(m,n)\right].\end{aligned} \tag{2.5}$$

Furthermore, in order to discuss vicinal surface with nonzero inclination, we add the terms of Andreev field[30] $\vec{\eta}=(\eta_x,\eta_y)$, which makes surface tilt, as follows:

$$\begin{aligned}\mathcal{H}_{\mathrm{vicinal}}&=\mathcal{H}_{\mathrm{RSOS-I}}-\eta_x\sum_{m,n}\left[h(m+1,n)-h(m,n)\right]\\&\quad-\eta_y\sum_{m,n}\left[h(m,n+1)-h(m,n)\right],\end{aligned} \tag{2.6}$$

where we have only the case with $\eta_x=\eta$ and $\eta_y=0$.

B. Lattice-gas representation for adsorbates

We can map the RSOS-I model to an equivalent RSOS-lattice-gas model by replacing each Ising variable σ with the lattice-gas (LG) variable $c\,[c=(\sigma+1)/2]$. The Hamiltonian of the RSOS-lattice-gas coupled system is obtained from the Hamiltonian (2.5) as follows:

$$\begin{aligned}\mathcal{H}_{\mathrm{RSOS-LG}}&=\sum_{m,n}\left[\tilde{\epsilon}\{1-\tilde{\alpha}c_y(m,n)\}|h(m+1,n)-h(m,n)|\right.\\&\quad\left.+\tilde{\epsilon}\{1-\tilde{\alpha}c_x(m,n)\}|h(m,n+1)-h(m,n)|\right]\\&\quad-4J\sum_{m,n}\left[c_x(m,n)c_y(m,n)+c_x(m,n)c_y\right.\\&\quad\times(m-1,n)+c_x(m,n-1)c_y(m,n)\\&\quad\left.+c_x(m,n-1)c_y(m-1,n)\right]\\&\quad-\mu\sum_{m,n}\left[c_x(m,n)+c_y(m,n)\right]+\mathrm{const},\end{aligned} \tag{2.7}$$

where

$$\tilde{\epsilon}=\epsilon(1+\alpha),\quad \tilde{\alpha}=\frac{2\alpha}{1+\alpha}, \tag{2.8}$$

$$\mu=2(H-J). \tag{2.9}$$

The $\tilde{\epsilon}$ describes the microscopic ledge energy of the ''clean,'' i.e., adsorbate-free, surface, μ the chemical potential of adsorbates, $4J$ the lateral bond energy between adsorbates, and $\tilde{\alpha}$ the microscopic interplay constant between adsorbates and the surface. Physically, H is related to the vapor pressure of adsorbates P as $H=(1/2)k_BT\ln P$.

Instead of making calculations for every combination of the values of the microscopic parameters, we show the calculations on the typical two cases with $\alpha>0$ and $J>0$, since our purpose of this paper is to clarify the origin of the thermal step bunching and the interstep attraction in the case of $J>0$.

Note that we can obtain the results for the case of $-\alpha$ directly from the results for the case of α, because the RSOS-I Hamiltonian remains unchanged by replacing $(\alpha,\sigma_x,\sigma_y,H)$ with $(-\alpha,-\sigma_x,-\sigma_y,-H)$.

III. STATISTICAL-MECHANICS CALCULATION WITH TRANSFER-MATRIX METHOD

The Andreev free energy $\tilde{f}(\eta)$[30] is calculated from the partition function Z as

$$\beta\tilde{f}(\eta)=-\lim_{N\to\infty}\frac{1}{N}\ln Z, \tag{3.1}$$

$$Z=\sum_{\{h(m,n)\}}\sum_{\{\sigma_x(m,n)\},\{\sigma_y(m,n)\}}e^{-\beta\mathcal{H}_{\mathrm{vicinal}}}, \tag{3.2}$$

where N is the number of lattice points of the RSOS system, $\beta=1/k_BT$, k_B the Boltzmann constant, and T the temperature. Physically, $\tilde{f}(\eta)$-η curve correspond to the section profile of the equilibrium crystal shape.[30] The system may undergo phase transition as the Andreev field is changed, to which we refer as the phase transition on the ECS.

In order to calculate Eq. (3.1) by the transfer-matrix method,[31] we map the RSOS-I Hamiltonian [(2.5) and (2.6)] to a decorated vertex model [Fig. 4(c)] or a 304-vertex

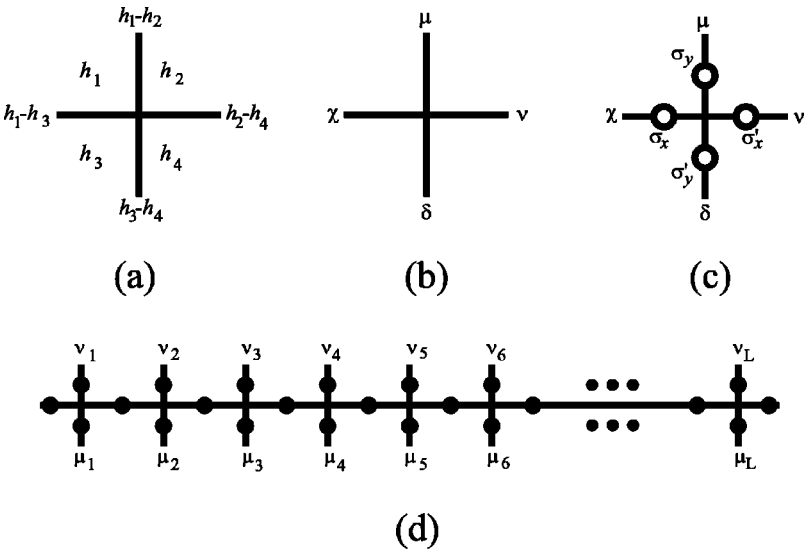

FIG. 4. (a) Top view of four nn columns on the RSOS lattice. (b) 19-vertex model. (c) The decorated vertex model. Ising spins are represented by circles. (d) Transfer matrix $\mathcal{T}$ represented by the decorated vertex model.

model.[23–25] The height differences between nn RSOS columns [Fig. 4(a)] are mapped to 19-vertex model [Fig. 4(b)], and the four Ising spins (circles) decorate the vertex [Fig. 4(c)]. Total number of allowed vertex configurations is then $19\times 2^4=304$. The statistical weight of each decorated-vertex configuration is obtained from the RSOS-I Hamiltonian [(2.5) and (2.6)].

In the transfer-matrix method, the problem is reduced to finding the largest eignevalue of the transfer matrix. For diagonalization of the transfer matrix, we employ the PWFRG algorithm,[19–21] whose efficiency has been well established.

The surface gradient $\vec{p}$ $(p_x=p, p_y=0)$ is obtained by the thermal average of the height difference as follows:

$$p(\eta)=\langle h(m+1,n)-h(m,n)\rangle a_z/a_x, \tag{3.3}$$

where $\langle\cdot\rangle$ expresses the thermal average, a_z (a_x) is the lattice constant for the z (x) direction. We set $a_z=a_x=1$, hereafter. By sweeping the field η, we obtain a p-η curve.

The magnetization M, the sublattice magnetization M_x and M_y are obtained by

$$M_x=\langle\sigma_x\rangle, \quad M_y=\langle\sigma_y\rangle,$$

$$M=(M_x+M_y)/2, \tag{3.4}$$

respectively.

The adsorption coverage Θ is calculated as

$$\Theta=(M+1)/2. \tag{3.5}$$

From the thermodynamics of the surface,[30,13] the surface-free energy per projected area $f(p)$ is calculated from the $\tilde{f}(\eta)$ by Legendre transformation as

$$f(p)=\tilde{f}(\eta)+\vec{p}\cdot\vec{\eta}, \tag{3.6}$$

where $\vec{\eta}=(\eta,0)$.

IV. STEPS WEAKLY COUPLED WITH ADSORBATES ($\alpha=0.1$)

A. Large J case

When J is large enough so that the order-disorder transition temperature exceeds the roughening transition temperature T_R of the terrace with adsorption, adsorption layer is always in the ordered state at the temperatures less than T_R, which means that the freedom of the adsorbates is frozen. Then the RSOS-I system reduced to the original RSOS system by the replacement of the microscopic ledge energy ϵ with $\epsilon^{\rm eff}=\epsilon(1-\alpha)$ $(H>0)$ or $\epsilon^{\rm eff}=\epsilon(1+\alpha)$ $(H<0)$. The roughening transition temperature of the terrace with adsorption is also given by Eq. (2.2) as $\epsilon^{\rm eff}/k_BT_R=0.633$.[27]

B. Medium J case: The first-order transition on the ECS

When J is not so large, the interplay between the surface system and the adsorbates system becomes significant. As a typical case, we take $J/\epsilon=0.25$ $(T_c\sim 0.5T_R)$. We have made statistical-mechanical calculation with the PWFRG algorithm in the case of $\alpha=0.1$, and $H/\epsilon=-0.02$.

At $k_BT/\epsilon=0.8$, we show η dependence of $-\tilde{f}(\eta)/k_BT$ [Fig. 5(a)] and $p(\eta)$ [Fig. 5(c)]; and we show p dependence of $f(p)/k_BT$ [Fig. 5(b)], and $M=2\Theta-1$ [Fig. 5(d)].

The curve of $-\tilde{f}(\eta)/k_BT$ is consistent with the GMPT universal behavior; $f(p)/k_BT$ has a cusp at $p=0$; p-η curve shows universal behavior of $p\propto\sqrt{\eta-\eta_c}$,[8–16,32–35] where η_c corresponds to the facet edge. Since we set $H<0$, the value of M at $p=0$ is negative; and then M increases continuously as p increases. Contrast to the case of $J=0$,[25] M_x is almost the same as M_y.

At $k_BT/\epsilon=0.55$, the calculated surface quantities are shown in Fig. 6. All the values of external parameters except temperature are the same as the values of parameters in Fig. 5.

The first-order transition on the[36–38,13] ECS is shown in the figure. There exist two ''branches'' in respective figures. One branch corresponds to the surface with the adsorption coverage $\Theta\sim 0$, and the other branch corresponds to the sur-

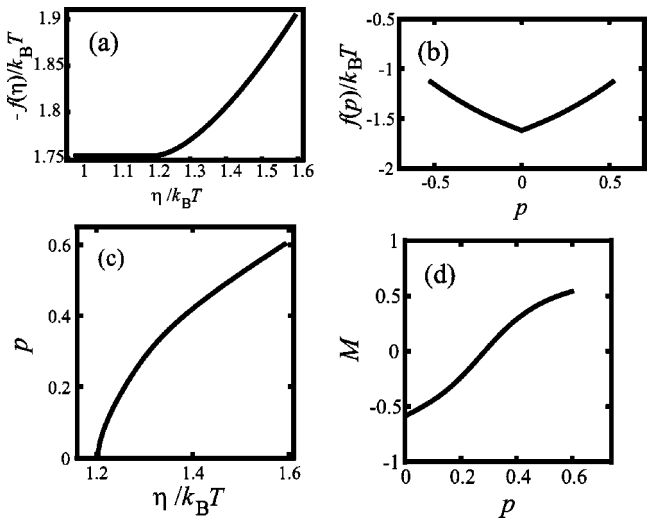

FIG. 5. Surface thermodynamical quantities calculated by PWFRG algorithm. $k_BT/\epsilon=0.8$, $\alpha=0.1$, $J/\epsilon=0.25$, and $H/\epsilon=-0.02$. (a) Andreev free energy $-\tilde{f}(\eta)/k_BT$ versus Andreev field η/k_BT. (b) Surface-free energy per projected area $f(p)/k_BT$ vs surface slope p. (c) p vs η/k_BT. (d) Mean magnetization $M=2\Theta-1$ vs p. Θ surface slope adsorption coverage.

face with $\Theta\sim1$. At $p=0$, the surface-free energy of the surface with $\Theta\sim0$ is lower than the one with $\Theta\sim1$; then the surface with $\Theta\sim0$ appears. The facet edge position is obtained from the two curves of the Andreev free energy as the cross point of the two curves. At the facet edge, the slope p jumps from 0 to a finite value p_1 at the facet edge on the ECS; and M also jumps from a negative value ($\Theta\sim0$) to a positive value ($\Theta\sim1$).

For some systems,[3,13,36–42] the form of $f(p)$ for the first-order transition is expected phenomenologically. Our present calculation gives the explicit form of $f(p)$ and $\Theta(p)$ from the microscopic model.

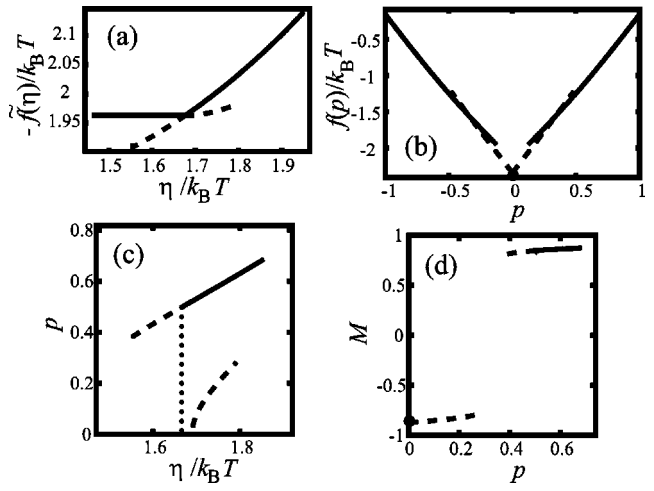

FIG. 6. Surface thermodynamical quantities calculated by the PWFRG algorithm. $k_BT/\epsilon=0.55$, $\alpha=0.1$, $J/\epsilon=0.25$, and $H/\epsilon=-0.02$. The dashed lines in (a), (c), and (d) shows the line for the metastable state. (a) $-\tilde{f}(\eta)/k_BT$ vs η/k_BT. (b) $f(p)/k_BT$ vs p. The branch with $\Theta\sim0$ is drawn by dashed line, while the branch with $\Theta\sim1$ is drawn by solid line. (c) p vs η/k_BT. (d) $M=2\Theta-1$ vs p.

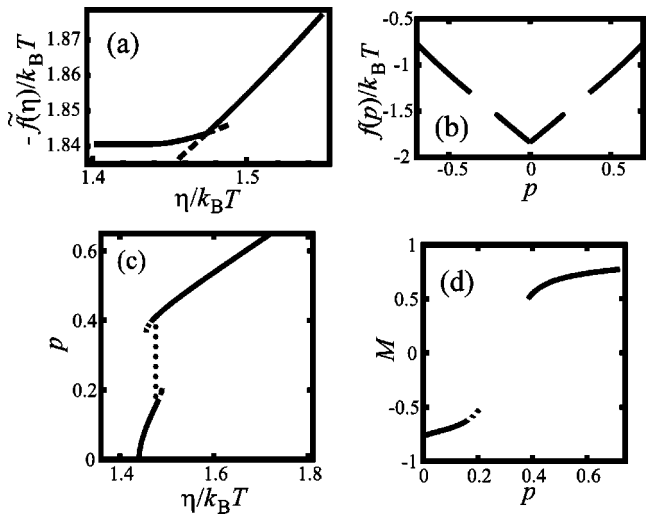

FIG. 7. Surface thermodynamical quantities calculated by the PWFRG algorithm. $k_BT/\epsilon=0.6$, $\alpha=0.1$, $J/\epsilon=0.25$, and $H/\epsilon=-0.02$. The dashed lines in (a), (c), and (d) show the lines for metastable states. (a) $-\tilde{f}(\eta)/k_BT$ vs η/k_BT. (b) $f(p)/k_BT$ vs p. (c) p vs η/k_BT. (d) $M=2\Theta-1$ vs p.

At $k_BT/\epsilon=0.6$, we show another case of the first-order transition in Fig. 7. At the facet edge, the GMPT behavior appears; while at a certain value of η, η_q, two curves of $-\tilde{f}(\eta)/k_BT$ crosses; then the slope p jumps from a lower value p_0 to an upper value p_1, and M also jumps. $f(p)$ curve contacts a tangential line at p_0 and p_1. There should be a region of $\partial^2 f(p)/\partial p^2<0$ in between p_0 and p_1, where the state would not be realized since the system is thermodynamically unstable.

At $k_BT/\epsilon=0.62$, we show surface quantities of a critical point $T_c(H)$ defined as the end of the first-order transition in Fig. 8. $k_BT_c(-0.02)/\epsilon$ is slightly higher than T_c ($k_BT_c/\epsilon\approx0.567$) for the pure 2D square Ising system.

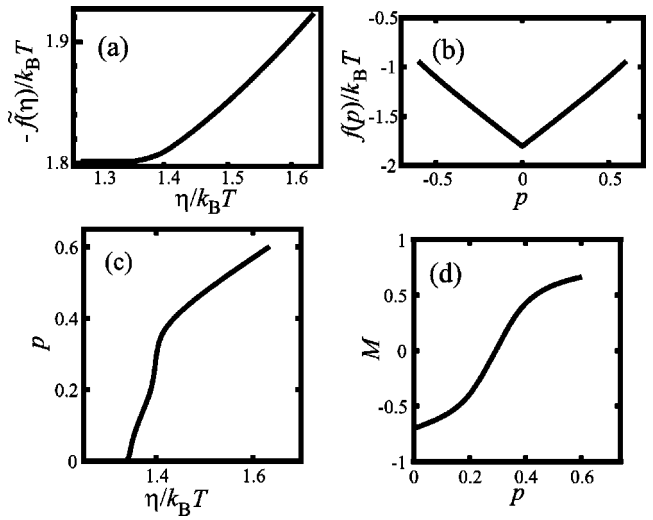

FIG. 8. Surface thermodynamical quantities calculated by the PWFRG algorithm. $k_BT/\epsilon=0.62$, $\alpha=0.1$, $J/\epsilon=0.25$, and $H/\epsilon=-0.02$. (a) $-\tilde{f}(\eta)/k_BT$ vs η/k_BT. (b) $f(p)/k_BT$ vs p. (c) p vs η/k_BT. (d) $M=2\Theta-1$ vs p.

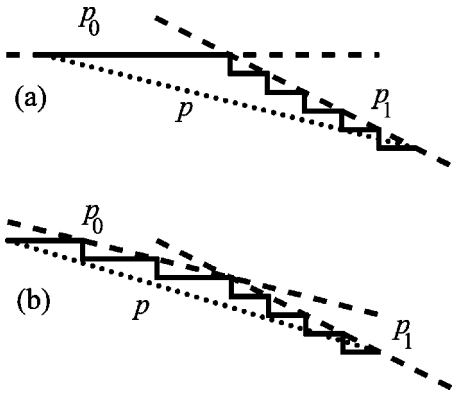

FIG. 9. The schematic figure for the surface separation with mean slope p. (a) $p_0=0$. (b) $p_0\neq 0$.

C. Thermal step bunching

When first-order transition on the surface occurs, two-phase coexistence occurs under the condition of a fixed mean slope. The surface with a slope p breaks up into two surfaces with the slope p_0 and the slope p_1 (Fig. 9). We call this separation of the surfaces as the thermal step bunching.

In the case of $p_0=0$ [Fig. 9(a)], the one of the separated surfaces is the singular surface and forms a wide terrace in the vicinal surface; the other of the separated surfaces with slope p_1 is formed by the bunching process of steps in the vicinal surface. Since the surface with slope p_1 is not the singular surface, we call the surface as a quasifacet. Note that the boundary between the surface with p_0 and the surface with p_1 is sharp; nevertheless, the quasifacet itself is rough, because $f(p)$ does not from the cusp singularity at $p=p_1$.

In the case of $p_0\neq 0$ [Fig. 9(b)], both of the separated surfaces are quasifacets.

From the thermodynamics of vicinal surface, we have following equations;[30]

$$p=-\partial\tilde{f}(\eta)/\partial\eta, \tag{4.1}$$

$$\eta=\partial f(p)/\partial p. \tag{4.2}$$

At the two-phase coexistence, we have

$$\tilde{f}(\eta(p_0))=\tilde{f}(\eta(p_1)),$$

$$\eta(p_0)=\eta(p_1)=\eta_q. \tag{4.3}$$

From Eq. (3.6) together with Eqs. (4.3), we have

$$f(p_1)-f(p_0)=\eta_q(p_1-p_0). \tag{4.4}$$

The equation Eq. (4.4) means that the $f(p)$ curve contacts with a tangential line with slope η_q at both points p_0 and p_1.

We show an example of the coexistent surfaces by Monte Carlo calculation in Fig. 1, where $p_0=0$. The surface made up of bunched 24 steps forms a quasifacet with the slope of p_1, and adsorbates segregate on the quasifacet.

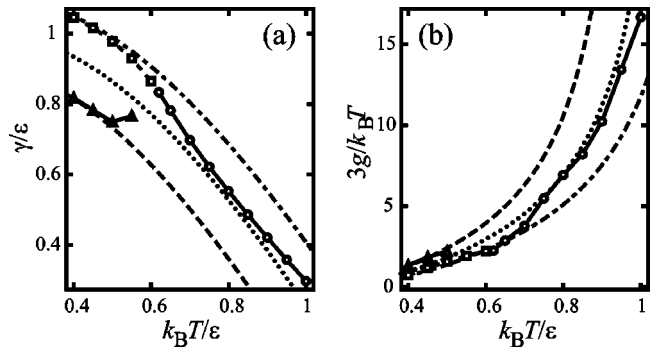

FIG. 10. $a_z=1$, $\alpha=0.1$, $J/\epsilon=0.25$, and $H/\epsilon=-0.02$. (a) Temperature dependence of step tension γ/ϵ. Solid line with open circles: The surface with adsorption in the disordered phase. Solid line with open triangles: Surface with the adsorption coverage $\Theta\sim 1$. Dashed line with open squares: Surface with the adsorption coverage $\Theta\sim 0$. The curves calculated from Eq. (4.8): $\epsilon^{\rm eff}=\epsilon$ (dotted), $\epsilon^{\rm eff}=0.9\epsilon$ (dashed), and $\epsilon^{\rm eff}=1.1\epsilon$ (dot dashed). (b) Step-interaction coefficient $3g/k_BT$. Solid line with open circles: The surface with adsorption in the disordered phase. Solid line with open triangles: Surface with the adsorption coverage $\Theta\sim 1$. Dashed line with open squares: Surface with the adsorption coverage $\Theta\sim 0$. The curves calculated from Eq. (4.9) with the universal relation Eq. (4.10): $\epsilon^{\rm eff}=\epsilon$ (dotted), $\epsilon^{\rm eff}=0.9\epsilon$ (dashed), and $\epsilon^{\rm eff}=1.1\epsilon$ (dot dashed).

D. Step tension and step stiffness

At lower temperatures than T_R, $f(p)$ takes the GMTP universal form[8–13] as follows:

$$f(p)=f(0)+\gamma|p|/a_z+g|p|^3+O(|p|^4), \tag{4.5}$$

where γ is the step tension, $a_z=1$ is the unit length of the step height, and g is the step interaction coefficient.

From Eqs. (4.2) and (4.5), η is obtained as

$$\eta=\gamma/a_z+3g|p|^2+O(|p|^3). \tag{4.6}$$

By assuming that η-p curve has the form of Eq. (4.6), we obtain step tension γ and step-interaction coefficient g from the least-square fitting of the calculated η-p curve to

$$\eta=A_0+A_2|p|^2+A_3|p|^3+A_4|p|^4. \tag{4.7}$$

The obtained step tension and step-interaction coefficient are shown in Figs. 10(a) and 10(b).

For $T<T_c(H)\approx 0.62\epsilon/k_B$, there are two branches in both γ and g; one branch corresponds to the step on the surface with the adsorption coverage $\Theta\sim 0$ and the other branch[43] corresponds to the step on the surface with $\Theta\sim 1$.

The two branches of γ converge to the curves of Ising approximation of the RSOS surface with $\epsilon^{\rm eff}=(1+\alpha)\epsilon=1.1\epsilon$ and $\epsilon^{\rm eff}=(1-\alpha)\epsilon=0.9\epsilon$, respectively, where the explicit forms of γ and the step stiffness $\tilde{\gamma}$ are given[23,44,45] as

$$\gamma=\epsilon^{\rm eff}+k_BT\ln[\tanh(\epsilon^{\rm eff}/2k_BT)], \tag{4.8}$$

$$\tilde{\gamma}=k_BT\sinh(\gamma/k_BT)=k_BT[\exp(\epsilon^{\rm eff}/k_BT)\tanh\{\epsilon^{\rm eff}/(2k_BT)\}$$
$$-\exp(-\epsilon^{\rm eff}/k_BT)\coth\{\epsilon^{\rm eff}/(2k_BT)\}]/2. \tag{4.9}$$

The two branches of g converges to the curves obtained from the step stiffness through the following universal relation;[14,15]

$$g a_z^3 = \frac{\pi^2}{6} \frac{(k_B T)^2}{\tilde{\gamma}}. \tag{4.10}$$

Therefore, the character of a single step is preserved, although the first-order transition occurs.

In the temperature region of $k_B T_c(H)/\epsilon < k_B T/\epsilon < 0.9$, the curve of γ and g converge to the ones calculated from 2D square Ising model with $\epsilon^{\rm eff} = \epsilon$. Since the adsorption layer is in the disordered phase with $\Theta \sim 0.5$, the adsorbates come randomly to the step ledge.

At higher temperatures than 0.9 ($k_B T/\epsilon > 0.9$), the values of γ shift upwards and the values of g shift downwards from the values of 2D Ising system with $\epsilon^{\rm eff} = \epsilon$. In this temperature region, the multilevel height configurations of the surface increases since γ decrease; then the multilevel objects block step deformation, which increases the step stiffness. In addition, the fluctuation of a single step is suppressed by the multilevel objects, entropy in the step free energy decreases, which increases γ.

V. FIELD-INDUCED FIRST-ORDER TRANSITION

In order to get intuitive insight for the origin of the first-order transition of the surface, we present a mean-field theory via Callen's identity.[46]

We choose a certain site $b = (m_b, n_b)$ on the lattice. We rewrite the Hamiltonian $\mathcal{H}_{\rm vicinal}$ [Eq. (2.6)] as follows:

$$\mathcal{H}_{\rm vicinal} = -\sigma_{x,b} H^{\rm eff}_{y,b}(|\Delta h_{y,b}|) + \text{others} \tag{5.1}$$

$$= -\sigma_{y,b} H^{\rm eff}_{x,b}(|\Delta h_{x,b}|) + \text{others}, \tag{5.2}$$

where

$$H^{\rm eff}_{y,b}(|\Delta h_{y,b}|) = J[\sigma_y(m_b, n_b) + \sigma_y(m_b - 1, n_b) + \sigma_y(m_b, n_b + 1) + \sigma_y(m_b - 1, n_b + 1)] + H + \alpha\epsilon |\Delta h_{y,b}|, \tag{5.3}$$

$$H^{\rm eff}_{x,b}(|\Delta h_{x,b}|) = J[\sigma_x(m_b, n_b) + \sigma_x(m_b + 1, n_b) + \sigma_x(m_b, n_b - 1) + \sigma_x(m_b + 1, n_b - 1)] + H + \alpha\epsilon |\Delta h_{x,b}|, \tag{5.4}$$

$$\Delta h_{x,b} = h(m_b + 1, n_b) - h(m_b, n_b),$$

$$\Delta h_{y,b} = h(m_b, n_b + 1) - h(m_b, n_b). \tag{5.5}$$

From Eqs. (5.3)–(5.5), the mean field acting on an adsorbate on the surface is

$$\langle H^{\rm eff}_{y,b} \rangle = 4JM_y + H + \alpha\epsilon \langle |\Delta h_y| \rangle, \tag{5.6}$$

$$\langle H^{\rm eff}_{x,b} \rangle = 4JM_x + H + \alpha\epsilon \langle |\Delta h_x| \rangle. \tag{5.7}$$

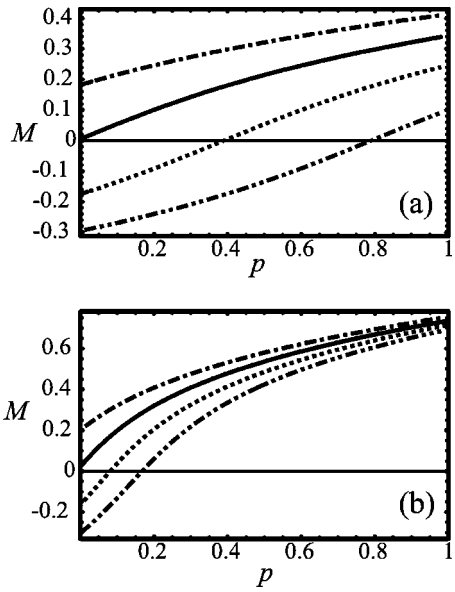

FIG. 11. Slope dependence of $M = 2\Theta - 1$ with $H/\epsilon = 0.02$ (dot dashed), 0 (solid), -0.02 (dotted), and -0.04 (two dots dashed). (a) $\alpha = 0.1$, $J/\epsilon = 0.25$, and $k_B T/\epsilon = 1.1$. (b) $\alpha = 0.5$, $J/\epsilon = 0.15$, and $k_B T/\epsilon = 0.7$.

Here, we have the relation $\langle |\Delta h_x| \rangle \approx p + \delta$ and $\langle |\Delta h_y| \rangle \approx \delta$. Therefore, when $\alpha > 0$, surface steps and surface roughness give rise to a positive effective field.

From the Callen Identity,[46]

$$\langle \sigma_{x,b} \rangle = \frac{1}{Z} \sum_{\{h\}} \sum_{\{\sigma_y\}} \sum_{\{\sigma_{x,b'}\}} \sum_{\sigma_{x,b}} \sigma_{x,b} e^{-\beta \mathcal{H}_{\rm vicinal}} = \langle \tanh[\beta H^{\rm eff}_{y,b}(|\Delta h_{y,b}|)] \rangle. \tag{5.8}$$

Note that $f(|\Delta h|) = f(0) + [f(1) - f(0)]|\Delta h|$ holds for arbitrary function f due to the RSOS condition ($\Delta h = 0, \pm 1$). We then rewrite right-hand side of Eq. (5.8)

$$\langle \sigma_{x,b} \rangle = \langle \tanh[\beta H^{\rm eff}_{y,b}(0)] \rangle + \langle [\tanh\{\beta H^{\rm eff}_{y,b}(0) + \beta\alpha\epsilon\} - \tanh\{\beta H^{\rm eff}_{y,b}(0)\}] |\Delta h_{y,b}| \rangle. \tag{5.9}$$

Using $\tanh X - \tanh Y = \sinh(X - Y)/(\cosh X \cosh Y)$, we obtain

$$\langle \sigma_{x,b} \rangle = \langle \tanh[\beta H^{\rm eff}_{y,b}(0)] \rangle + \sinh(\beta\alpha\epsilon) \left\langle \frac{|\Delta h_{y,b}|}{Q} \right\rangle, \tag{5.10}$$

$$\langle \sigma_{y,b} \rangle = \langle \tanh[\beta H^{\rm eff}_{x,b}(0)] \rangle + \sinh(\beta\alpha\epsilon) \left\langle \frac{|\Delta h_{x,b}|}{Q'} \right\rangle, \tag{5.11}$$

$$Q = \cosh[\beta H^{\rm eff}_{y,b}(0) + \beta\alpha\epsilon] \cosh[\beta H^{\rm eff}_{y,b}(0)], \tag{5.12}$$

$$Q' = \cosh[\beta H^{\rm eff}_{x,b}(0) + \beta\alpha\epsilon] \cosh[\beta H^{\rm eff}_{x,b}(0)]. \tag{5.13}$$

For the better mean-field approximation, we use Eqs. (5.10) and (5.11). We approximate $\langle |\Delta h_{y,b}|/Q \rangle$ as

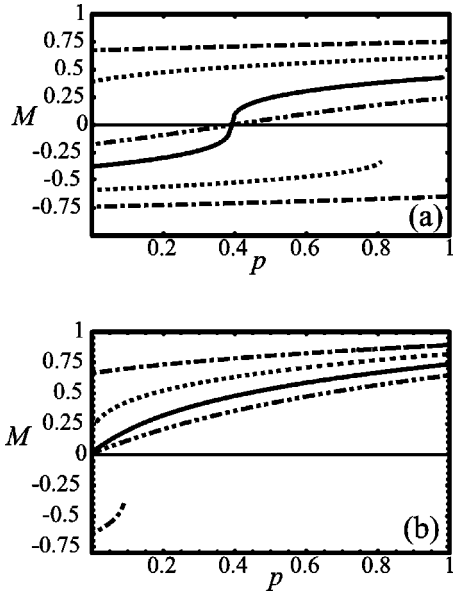

FIG. 12. Slope dependence of $M=2\Theta-1$ for several temperatures. (a) $H/\epsilon=-0.02$, $\alpha=0.1$, and $J/\epsilon=0.25$. $k_{\mathrm{B}}T/\epsilon=0.8$ (dot dashed), 0.9 (dotted), 1.0 (solid), and 1.1 (two dots dashed). (b) $H/\epsilon=0$, $\alpha=0.5$ and $J/\epsilon=0.15$. $k_{\mathrm{B}}T/\epsilon=0.5$ (dot dashed), 0.6 (dotted), 0.7 (solid), and 0.8 (two dots dashed).

$$\left\langle \frac{|\Delta h_{y,b}|}{Q} \right\rangle = \frac{\langle |\Delta h_{y,b}| \rangle}{\langle Q \rangle}. \tag{5.14}$$

We have, from Eqs. (5.10) and (5.11), the self-consistent equations in the mean-field approximation:

$$M_x = \tanh(4\beta J M_y + \beta H) + \sinh(\beta\alpha\epsilon)\frac{\delta}{\tilde{Q}}, \tag{5.15}$$

$$M_y = \tanh(4\beta J M_x + \beta H) + \sinh(\beta\alpha\epsilon)\frac{p+\delta}{\tilde{Q}'}, \tag{5.16}$$

$$\tilde{Q} = \cosh[(4\beta J M_y + \beta H) + \beta\alpha\epsilon]\cosh(4\beta J M_y + \beta H), \tag{5.17}$$

$$\tilde{Q}' = \cosh[(4\beta J M_x + \beta H) + \beta\alpha\epsilon]\cosh(4\beta J M_x + \beta H). \tag{5.18}$$

We introduce quantities M and Δ as

$$M=(M_x+M_y)/2, \quad \Delta=(M_y-M_x)/2. \tag{5.19}$$

Since $\delta\approx 0$ for low T, Eqs. (5.15) and (5.16) become

$$M = \frac{\sinh[8\beta J M + 2\beta H]}{2\tilde{Q}''} + p\frac{\sinh(\beta\alpha\epsilon)}{2\tilde{Q}'}, \tag{5.20}$$

$$\Delta = \frac{\sinh[-8\beta J\Delta]}{2\tilde{Q}''} + p\frac{\sinh(\beta\alpha\epsilon)}{2\tilde{Q}'}, \tag{5.21}$$

$$\tilde{Q}' = \cosh[4\beta J(M-\Delta)+\beta H+\beta\alpha\epsilon] \times \cosh[4\beta J(M-\Delta)+\beta H], \tag{5.22}$$

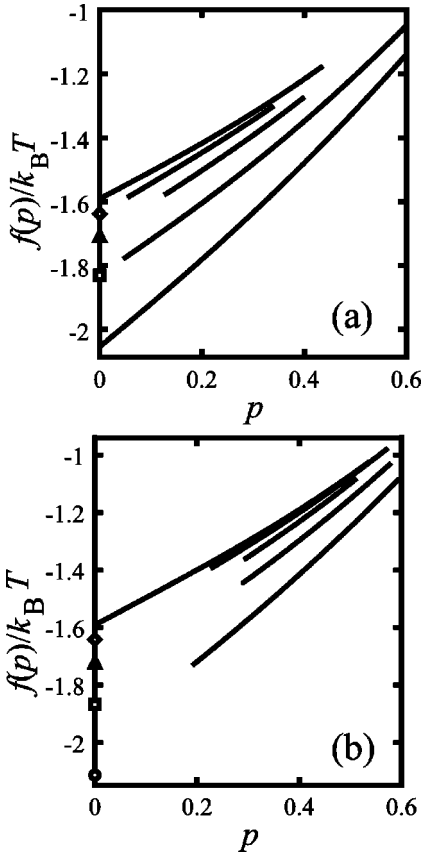

FIG. 13. $f(p)$-p curves. $\alpha=0.5$ and $J/\epsilon=0.15$. Temperatures of the curves are $k_{\mathrm{B}}T/\epsilon=0.5$, 0.45, 0.4, 0.35, and 0.3 from the top to the bottom. Values at $p=0$ are shown by symbols for $k_{\mathrm{B}}T/\epsilon=0.45$ (open diamond), 0.4 (open triangle), 0.35 (open square), and 0.3 (open circle). (a) $H=0$. (b) $H/\epsilon=-0.01$.

$$\tilde{Q}'' = \cosh[4\beta J(M-\Delta)+\beta H]\cosh[4\beta J(M+\Delta)+\beta H]. \tag{5.23}$$

In Fig. 11 and Fig. 12, we show M-p curve obtained by the numerical solution of Eqs. (5.20) and (5.21) with $\delta=0$.

Note that $|\Delta|\ll 1$ for $J>0$. Eqs. (5.20) and (5.21), then, become

$$M = \tanh(4\beta J M + \beta H) + p\frac{\sinh(\beta\alpha\epsilon)}{2\tilde{Q}'}, \tag{5.24}$$

$$\Delta = \frac{\cosh(4\beta J M + \beta H)}{\cosh^2(4\beta J M + \beta H) + 4\beta J} p \times \frac{\sinh(\beta\alpha\epsilon)}{2\cosh(4\beta J M + \beta H + \beta\alpha\epsilon)}. \tag{5.25}$$

The mean-field critical temperature T_c^{MF} for the "pure" 2D Ising system ($H=0$, $\alpha=0$) is $4J/k_{\mathrm{B}}T_{\mathrm{c}}{}^{\mathrm{MF}}=1$. For $T>T_{\mathrm{c}}{}^{\mathrm{MF}}$, regarding $\beta\ll 1$ and $\tilde{Q}'\sim\tilde{Q}''\sim 1$, we approximate further the Eqs. (5.24) and (5.25) as

$$M = \frac{\beta\epsilon}{1-4\beta J}[H/\epsilon + p\alpha/2], \tag{5.26}$$

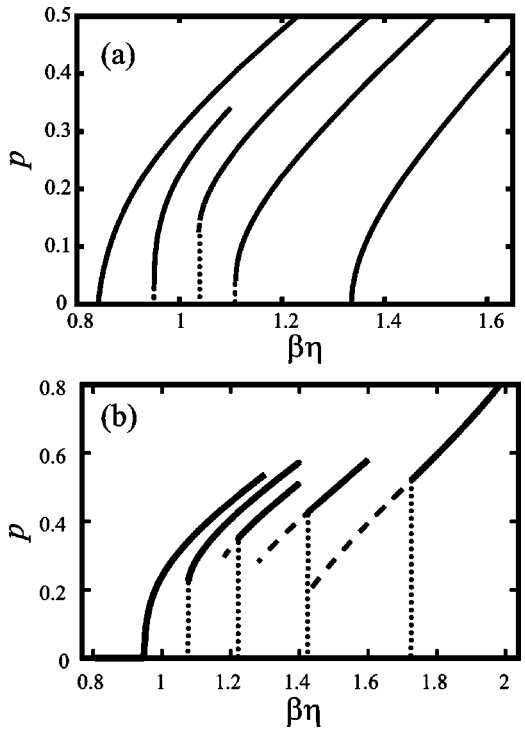

FIG. 14. p-$\beta\eta$ curves ($\alpha=0.5$ and $J/\epsilon=0.15$), where $\beta=1/k_BT$. Temperatures of curves are $k_BT/\epsilon=0.3$, 0.35, 0.4, 0.45, 0.5, and 0.55, from the right to the left. Dashed line: The values for metastable state. (a) $H=0$. (b) $H/\epsilon=-0.01$.

$$\Delta=\frac{\beta\epsilon}{1+4\beta J}p\alpha/2. \tag{5.27}$$

Therefore, for $\alpha>0$, M and Δ increase linearly as p increases; and the rate of the increase is proportional to α. We can see this from Fig. 11 clearly.

For $T<T_c^{\mathrm{MF}}$, the first-order transition occurs in M-p curve. There are two solutions for the Eq. (5.24); the one corresponds to the equilibrium state and the other to the metastable state. We show M-p curves for several temperatures in Fig. 12.

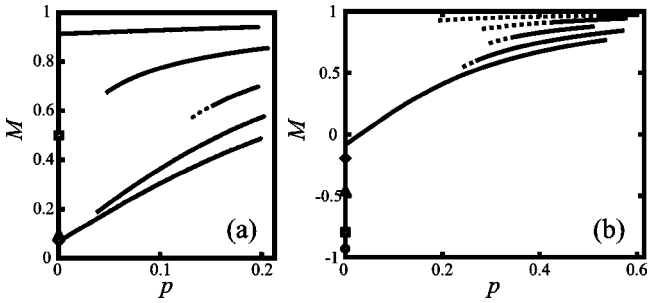

FIG. 15. $M-p$ curves ($\alpha=0.5$ and $J/\epsilon=0.15$). Temperatures of curves are $k_BT/\epsilon=0.3$, 0.35, 0.4, 0.45, 0.5, and 0.55, from the top to the bottom. The values at $p=0$ are shown by symbols for $k_BT/\epsilon=0.45$ (open diamond), 0.4 (open triangle), 0.35 (open square), and 0.3 (open circle). Dotted line: The values for metastable state. (a) $H=0$. (b) $H/\epsilon=-0.01$.

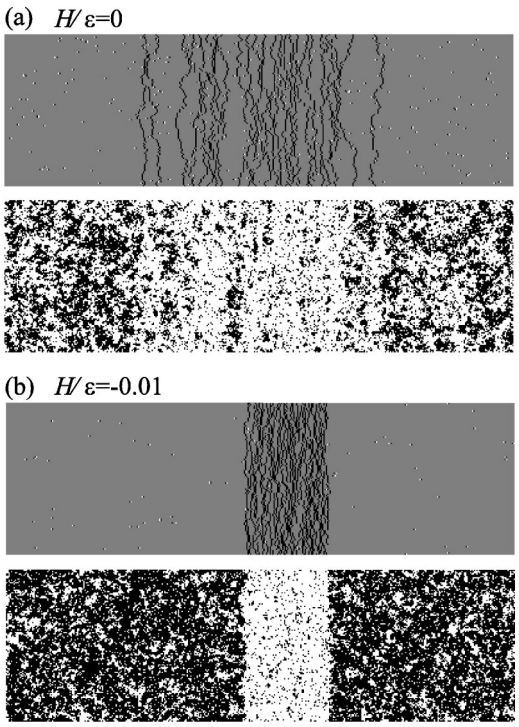

FIG. 16. An example of the top view of the RSOS-I surface: the snapshot on Monte Carlo simulation at 7×10^6 MCS. $\alpha=0.5$, $J/\epsilon=0.15$, and $k_BT/\epsilon=0.4$. Above: the configuration of the RSOS vicinal surface, where a white (black) point designate $h(m+1,n)-h(m,n)=\Delta_x(m,n)=1(-1)$. Below: the configuration of Ising system (adsorption layer), where white dots represent up spins (adsorbates). The RSOS system is covered with the adsorption system. Size: 408×120. Number of step = 24. (a) $H/\epsilon=0$. (b) $H/\epsilon=-0.01$.

This first-order transition is similar to the field-induced first-order transition in the ferromagnetism. In the case of $H<0$, as we can see from Eq. (5.4), $M<0$ at $p=0$. As η increases, p increases; then H^{eff} increases from a negative value to a positive value. This sign change of the H^{eff} cause the abrupt change between the ordered states, which we call the *field-induced first-order transition*. When $H\geqslant0$, M is always positive for every p. Therefore, the first-order transition never occurs.

VI. STEPS STRONGLY COUPLED WITH ADSORBATES ($\alpha=0.5$)

When α increases, the interplay between surface steps and adsorbates becomes larger. We give the PWFRG results in the case of $\alpha=0.5$, $J/\epsilon=0.15$, and for $H/\epsilon=0$, and -0.01 in Figs. 13–15.

In Fig. 13, we show surface-free energy $f(p)$ as the function of p. η-p curves and M-p curves are given in Figs. 14 and 15, respectively. The Monte Carlo results are also shown in Fig. 16.

Similar to the case of the small α, the first-order transition occurs for $H<0$. In the p-η curve, p always jumps from $p_0=0$ to $p=p_1(T,H)$. This means that the thermal step bunching of the type shown in Fig. 9(b) does not occur.

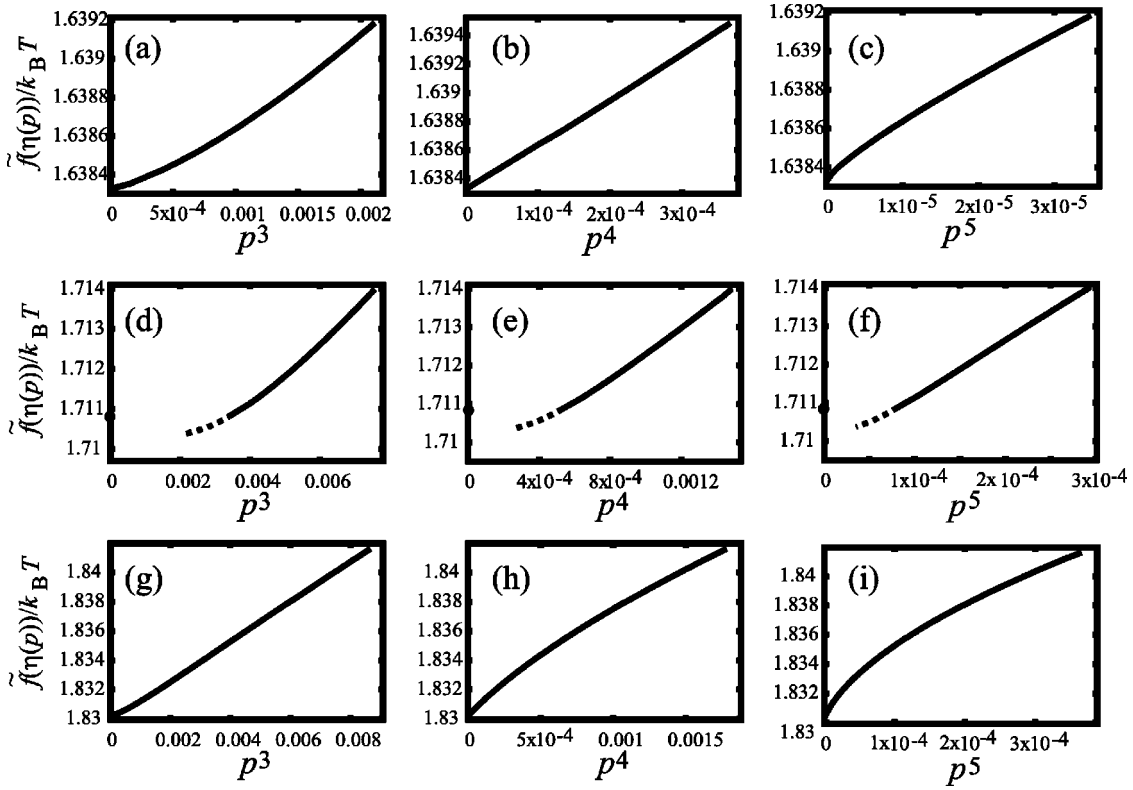

FIG. 17. $-\tilde{f}(\eta(p))/k_BT$-p^u curve, where $u=3$, 4, and 5. $\alpha=0.5$, $J/\epsilon=0.15$, and $H=0$. (a), (b), and (c) $k_BT/\epsilon=0.45$. (d), (e), and (f) $k_BT/\epsilon=0.4$. (g), (h), and (i) $k_BT/\epsilon=0.35$. Dotted line: values for the metastable state.

What is remarkable for strong-coupling case is that the first-order transition occurs even for positive H (≈ 0) in a temperature range near $k_BT/\epsilon \approx 0.4$ (which is close to the critical temperature $T_c \approx 0.340$ of the ''pure'' Ising system). Since there may not occur the sign change of the effective field for $H>0$ case, the explanation given in the preceding section cannot be applied to this type of the first-order transition. We may call this type of first-order transition as ''fluctuation-induced'' transition.

There exists two end points ($k_BT/\epsilon=0.45$ and $k_BT/\epsilon=0.35$) of the fluctuation-induced first-order transition. At theses points, there occurs the second-order transition. Interestingly, we have found that $f(p)$ does not take the well-known GMPT form at these points.

In order to see this, we draw $-\tilde{f}(\eta(p))/k_BT$-p^u curve in Fig. 17. From Eqs. (3.6), (4.5), and (4.6), we obtain

$$\tilde{f}(\eta(p))=f(0)-2g|p|^3-3g_4|p|^4-4g_5|p|^5+O(|p|^6), \tag{6.1}$$

where we have expanded $f(p)$ as

$$f(p)=f(0)+\gamma|p|/a_z+g|p|^3+g_4|p|^4+g_5|p|^5+O(|p|^6). \tag{6.2}$$

From the figures, the linearity of the curve is the best when $u=4$ at $k_BT/\epsilon=0.45$ and $k_BT/\epsilon=0.35$. g seems to vanish at the end point of the fluctuation-induced first-order transition.

VII. ADSORBATE-MEDIATED INTERSTEP ATTRACTION

A. Interstep attraction caused by density fluctuation of adsorbates

We show that the density fluctuation of adsorbates give rise to short-ranged attractive interaction between the steps.

In the coarse-grained description, the Ising part $\mathcal{H}_{\rm Ising}$ and the interaction part $\mathcal{H}_{\rm int}$ in the Hamiltonian (2.5) can be written as[46,47] (in the Gaussian approximation for the Ising field);

$$\mathcal{H}_{\rm Ising}=\int d^2x\left\{\frac{1}{2}[\vec{\nabla}\phi(x)\vec{\nabla}\phi(x)+\mu_m^2\phi^2(x)]\right\},$$

$$\mathcal{H}_{\rm int}=-\alpha\epsilon\int d^2x\,\phi(x)|\vec{\nabla}_x\tilde{h}|, \tag{7.1}$$

where the field $\phi(x)$ denotes the local deviation of magnetization from its mean values on the terrace, μ_m is the ''mass,'' $\tilde{h}(x)$ is the ''height field,'' and ∇_x is the derivative along the x direction.

After performing the integration with respect to the field $\{\phi(x)\}$ as,

$$\int \mathcal{D}\phi\,\exp[-\beta(\mathcal{H}_{\rm Ising}+\mathcal{H}_{\rm int})]\sim\exp[-\beta\mathcal{H}_{\rm step}], \tag{7.2}$$

we obtain the effective Hamiltonian as

$$\mathcal{H}_c^{\rm eff}=\mathcal{H}_{\rm RSOS}+\mathcal{H}_{\rm step}. \tag{7.3}$$

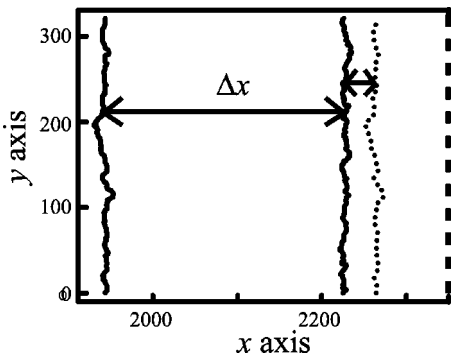

FIG. 18. An example of the step configuration with two steps. $\alpha=0.5$, $J=0.15$, $H/\epsilon=0.005$, and $k_BT/\epsilon=0.4$. Size of the system: 320×320. Time: 1×10^7 MCS/site. We adopt periodic boundary condition; the system is replicated in y direction and in x direction, where the surface height is added by 2 (-2) for the replica system in x $(-x)$ direction. The dotted curve shows the step on the left side in the replicated system.

The second term $\mathcal{H}_{\rm step}$ is the Hamiltonian for the interaction between steps given as

$$\mathcal{H}_{\rm step}=-\,{\rm const}(\alpha\epsilon)^2\int d^2y\int d^2x' \times|\nabla_x h(y)|\frac{1}{-\nabla^2+\mu_m^2}|\nabla_x h(x')|, \qquad (7.4)$$

where $[-\nabla^2+\mu_m^2]^{-1}$ is calculated by way of Fourier transformation; we obtain the term which amounts to the exponentially decaying form $\exp(-\mu_m|y-x|)$ of the interaction.

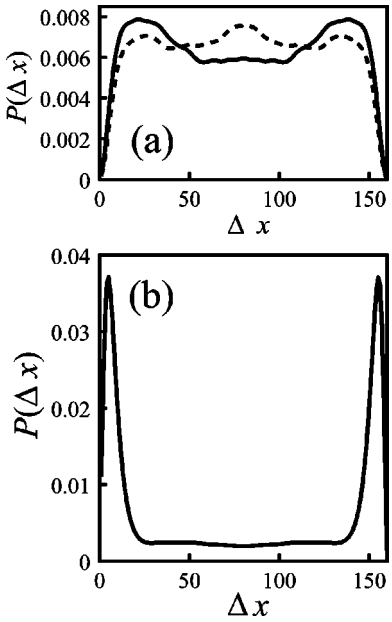

FIG. 19. The two-step terrace width distribution function. Size: 160×160. (a) $\alpha=0.1$, $H/\epsilon=-0.02$, and $k_BT/\epsilon=0.5$. Time: 2×10^8 MCS/site. Solid line: $J=0.25$. Dashed line: $J=0$. (b) $\alpha=0.5$, $J=0.15$, $H/\epsilon=-0.01$, and $k_BT/\epsilon=0.4$. Time: 1×10^8 MCS/site.

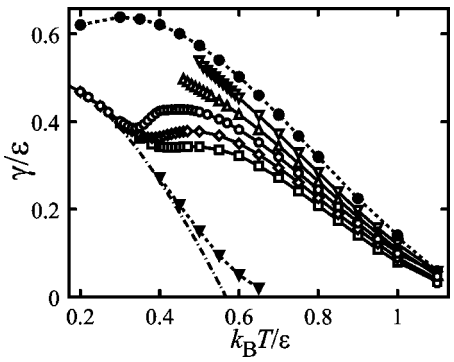

FIG. 20. Temperature dependence of step tension γ/ϵ obtained by the least-square fitting of the PWFRG results to Eq. (4.7) with Eq. (4.6), where we set $a_z=1$, $\alpha=0.5$, and $J/\epsilon=0.15$. $H/\epsilon=-0.02$ (line with the reversed open triangle), -0.01 (line with the open triangle), 0 (line with the open circle), 0.01 (line with the open diamond), and 0.02 (line with the open square). Dotted line with closed circles: $J=0$, $H=0$, and $\alpha=0.5$. Dotted line with the reversed closed triangles: the step tension of the original RSOS system with $\epsilon^{\rm eff}=0.5\epsilon$ obtained by the PWFRG algorithm. Dash dotted line: the step tension calculated from Eq. (4.8) with $\epsilon^{\rm eff}=0.5\epsilon$.

Therefore, adsorbate-mediated step interaction is of short ranged, and the strength of the adsorption is proportional to α^2. Note that the sign in front of the integral is always minus implying that the interaction is attractive.

We think this interstep attraction is the origin of the fluctuation-induced first-order transition mentioned in the preceding section.

B. Terrace width distribution

To confirm the interstep attraction in the RSOS-I system, we have made Monte Carlo calculations. We study the terrace width distribution function of the surface with two steps (Fig. 18). In Fig. 19, the two-step terrace width distribution function are shown for $\alpha=0.1$ and $\alpha=0.5$. The value of parameters are chosen so that the field-induced (for $\alpha=0.1$) first-order transition or the fluctuation-induced (for $\alpha=0.5$) first-order transition occurs.

For $\alpha=0.1$, double broad peaks are seen in the terrace width distribution, which can be attribute to the weak interstep attraction. The attraction is not strong enough to cause thermal bunching.

For $\alpha=0.5$, there are two sharp peaks, and we have confirmed that the peak width is essentially independent of the system size. The off-peak values of the distribution reduce to zero in the large system size limit. Thus, the steps form a bound state due to adsorbate-mediated interstep attraction.

C. Step tension and step-interaction coefficient

For $\alpha=0.5$, we obtained step tension γ and step-interaction coefficient g by the least square fitting of the calculated p-η curve Eq. (4.7). We shows the results in Figs. 20 and 21.

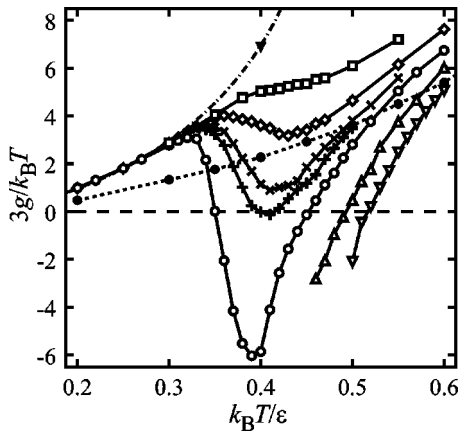

FIG. 21. Temperature dependence of the step-interaction coefficient $3g/k_BT$ obtained from the least-square fitting of the PWFRG results to Eq. (4.7) with Eq. (4.6). $a_z=1$, $\alpha=0.5$, and $J/\epsilon=0.15$. $H/\epsilon=-0.02$ (line with the reversed open triangle), -0.01 (line with the open triangle), 0 (line with the open circle), 0.0035 (line with $+$), 0.005 (line with $\times$), 0.01 (line with the open diamond), and 0.02 (line with the open square). Dotted line with closed circles: $J=0$, $H=0$, and $\alpha=0.5$. Reversed closed triangle: the step-interaction coefficient of the original RSOS system with $\epsilon^{\rm eff}=0.5\epsilon$ obtained by the PWFRG algorithm. Dash dotted line: the step-interaction coefficient calculated from Eq. (4.9) with $\epsilon^{\rm eff}=0.5\epsilon$ together with the universal relation Eq. (4.10).

In the lower temperature than $T_c\approx 0.34$, and for $H\geqslant 0$, γ and g converge to the RSOS one with $\epsilon^{\rm eff}=0.5\epsilon$, since $M(\Theta)\approx 1$. When $H<0$, the field-induced first-order transition occurs.

In the temperature region $T_c<T<0.6\epsilon/k_B$, γ and g show interesting behavior. When $H/\epsilon<0.0035$, the fluctuation-induced first-order transition occurs. As we decrease temperature from $T\approx 0.6\epsilon/k_B$, g obtained by the least-square fitting decreases continuously; then g becomes negative, where the first-order transition occurs. For $0\leqslant H/\epsilon\leqslant 0.0035$, further decrease in the temperature cause the increase of g, leading finally to positive g. At the end points of the first-order transition, $T_{s,l}$ and $T_{s,u}$, g becomes zero[24,25] ($k_BT_{s,l}/\epsilon\approx 0.35$ and $k_BT_{s,u}/\epsilon\approx 0.45$ in the case of $H=0$).

As for the case of $0.0035<H/\epsilon<0.02$, γ shows the quasireentrant step behavior.[48] One simple possible explanation for the vanishing of g at $T_{s,l}$ and $T_{s,u}$, might be given in terms of the ''single-step'' mechanism; due to Eq. (4.10), vanishing of g implies divergence of step stiffness $\tilde{\gamma}$. As a check for this mechanism, we have made the Monte Carlo calculation of the scaled single-step fluctuation width σ, which is related to $\tilde{\gamma}$ as

$$\sigma^2=\frac{k_BT}{\tilde{\gamma}}. \tag{7.5}$$

The calculated σ^2 is finite and monotonically increasing for $0.35\leqslant k_BT/\epsilon\leqslant 0.55$ (Fig. 22). Hence, $\tilde{\gamma}$ does not show divergent behavior, which rejects the single-step mechanism.

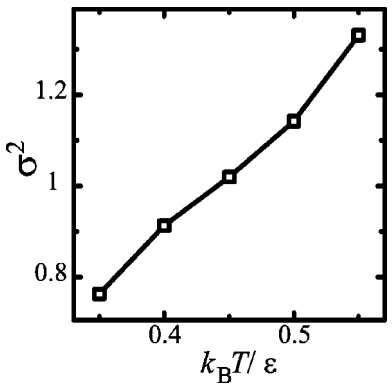

FIG. 22. Temperature dependence of the fluctuation width of a single step (Monte Carlo calculation). $\alpha=0.5$, $J/\epsilon=0.25$, and $H/\epsilon=0.005$. Size: 160×160. Average time: 6×10^6 MCS/site.

D. Step-droplet picture

Recall that, in the derivation of the universal relation Eq. (4.10), it is assumed that the steps do not form bound states. In our case, as has been discussed in the preceding section, there arises interstep attraction due to the density fluctuation of the adsorbate. If the attraction is strong enough, the steps may form bound states, which invalidate the ''single-step'' universal relation Eq. (4.10). We present here an argument for the vanishing of g in terms of the bound steps.

Assume that step form n-body bound states. By ρ_n, we denote the density of the n-body bound step (by ρ_1, we denote the ordinary nonbounded step density). Since each bunch of n-bound steps can be regarded as a single multiple-height step, the system of n-bound steps may be again in the GMPT universality class. Hence, we have the following expansion of the vicinal-surface-free energy f:

$$f=\gamma_n\rho_n+B_n\rho_n^3+(\text{higher-order tems}), \tag{7.6}$$

with

$$B_n=\frac{\pi^2}{6}\frac{(k_BT)^2}{\tilde{\gamma}_n}, \tag{7.7}$$

where γ_n is the step tension of the n-bound step, and $\tilde{\gamma}_n$ the corresponding stiffness ($\gamma_1=\gamma, \tilde{\gamma}_1=\tilde{\gamma}$).

Note that, roughly (in the order-of-magnitude estimation), we have[49]

$$\gamma_n\sim n\gamma_1, \tag{7.8}$$

$$\tilde{\gamma}_n\sim n\tilde{\gamma}_n, \tag{7.9}$$

which leads to

$$B_n\sim\frac{1}{n}B_1. \tag{7.10}$$

Since the surface gradient $|\vec{p}|$ relates to ρ_n as

$$|\vec{p}| = n\rho_n a_z . \tag{7.11}$$

We have $[\rho_n = |\vec{p}|/(na_z) = \rho_1/n]$

$$f = \gamma_n \rho_n + B_n \rho_n^3 (+ \text{higher-order terms})$$

$$\sim \gamma_1 \rho_1 + \frac{1}{n^4} B_1 \rho_1^3 \tag{7.12}$$

$$= \gamma_1 |\vec{p}|/a_z + g|\vec{p}|^3, \tag{7.13}$$

with

$$g = \frac{B_1}{n^4 a_z^3}. \tag{7.14}$$

Hence, g can vanish if n diverges: $g \to 0$ $(n \to \infty)$.

In the above argument, we have fixed n. There may, however, the cases where the value of n is distributed in a range. In other words, steps form ''droplets'' with mean droplet size $\langle n \rangle$ (See Fig. 16). In such cases, we should modify Eq. (7.14) to

$$g \sim \frac{B_1}{\langle n \rangle^4 a_z^3}, \tag{7.15}$$

which also vanished as the mean droplet size $\langle n \rangle$ diverges. We think that this step-droplet picture gives a valid explanation for the vanishing of g at $T_{s,l}$ and $T_{s,u}$.

Seemingly similar n-body bound step have appeared in the discussion of ''quantum n-mer.''[50] In Ref. 50, it has been shown that energy balance between the long-range (elastic) repulsion and the short-range attraction leads to formation of stable n-bound steps (quantum n-mers). We may refer to this mechanism of the formation of bound step as the *energy origin*. In contrast, our mechanism may be referred to as the *entropy origin*, because the short-ranged attraction itself is generated by fluctuation of the adsorbates density.

VIII. APPLICATION TO REAL SYSTEMS

Let us briefly comment on the relevance of the present work to existing experimental observations. Adsorption-induced faceting or step bunching has been reported in various systems.[3,51–61] For some systems, the faceting or the step bunching has been reversible upon adsorbate adsorption/desorption, which suggest that the adsorption-induced step bunching is of thermodynamic origin. For example, the giant step formation observed for Au on Si(001) surface[51,52] is understood as the thermal step bunching of the field-induced type, which we have been proposed in the present paper. Au atoms on Si(001) have attractive lateral interaction among themselves, suggesting that $J>0$; Au atoms avoid ledge of the step on the surface,[52] which suggests $\alpha<0$. The macrostep formation observed for Ga/Si(111) system[60] may also be understood as the field-induced first-order transition. Ga atom favors the step ledge,[60] and changes step energy,[60] which suggests $\alpha>0$. It is known that chemisorbed oxygen on[54] Ag(331) or Ag(110) causes[53] faceting, which is reversible upon O_2 adsorption and desorption. Ozcomert *et al.* observed the vicinal surface of O/Ag(110) system,[53] and they gave a phenomenological form of $f(p)$. Their $f(p)$ is quite similar to our $f(p)$ curve in case of $\alpha=0.5$, $J=0.15$, $H=0$, and $k_B T/\epsilon \sim 0.4$. Therefore, the system may possibly be a realization of the step bunching due to the adsorbate-mediated interstep attraction.

IX. SUMMARY

We have studied the interplay between the vicinal surface and the adsorption below the roughening temperature. In this paper, we have clarified the origin of the thermal step bunching or the quasifacet formation by making detail calculation on the surface thermodynamical quantities.

We have presented the restricted solid-on-solid model coupled with the Ising model (RSOS-I model) on the square lattice [Eqs. (2.5) and (2.6)]. The coverage (Θ) of the adsorption is assumed to be less than 1, and the surface height difference between nn site is restricted to $\{0,\pm 1\}$. We have introduced the coupling constant α between the surface and the adsorbates. Small α corresponds to the physisorption system, and large α corresponds to the chemisorption system. We have concentrated on the case of the attractive lateral interaction between adsorbates $(J>0)$.

We have calculated, by the transfer-matrix method, the Andreev free energy $\tilde{f}(\eta)$, p-η curves (p is the surface slope, and η is the Andreev field), and M-p curves ($M=2\Theta-1$). As an efficient computational algorithm, we adopt the PWFRG algorithm[19] which is a variant of the DMRG algorithm.[17]

The surface-free energy per projected area $f(p)$ is calculated from the Andreev free energy $\tilde{f}(\eta)$ by the Legendre transformation. Step tension γ and step-interaction coefficient g are obtained from the least-square fitting of the calculated p-η curves to the GMPT universal form of $f(p)$.

For steps weakly coupled with adsorbates $(\alpha=0.1)$, the field-induced first-order transition occurs as Andreev field η changes, where the surface slope p assumes a finite jump. This field-induced first-order transition occurs for $T<T_c$ and $H<0$, where T_c is the critical temperature of the 2D Ising system, and H is the magnetic field connecting to the chemical potential of the adsorbates μ as $H=\mu/2+J$.

For steps strongly coupled with adsorbates $(\alpha=0.5)$, the fluctuation-induced first-order transition occurs. This fluctuation-induced first-order transition occurs for $T \sim T_c$, which occurs even at positive H. The origin of the fluctuation-induced first-order transition is the adsorbate-mediated interstep attraction caused by the density fluctuation of adsorbates on the surface.

For positive H, at the end points of the fluctuation-induced first-order transition, the step-interaction coefficient

g vanishes. This vanishing *g* phenomena has been explained in terms of the step-droplet picture.

The phenomena of the step bunching have usually been discussed under the nonequilibrium conditions such as the electromigration.[62] We would like to stress that the adsorption-induced bunching or the quasifacet formation discussed in the present paper is an equilibrium phenomenon, giving a mechanism of the step bunching.

ACKNOWLEDGMENTS

This work was partially supported by the ''Research for the Future'' Program from The Japan Society for the Promotion of Science (Grant No. JSPS-RFTF97P00201) and by the Grant-in-Aid for Scientific Research from Ministry of Education, Science, Sports, and Culture (Grant No. 09640462).

[1] M.C. Desjonquéres and D. Spanjaard, *Concepts in Surface Physics*, 2nd ed. (Springer-Verlag, Berlin, 1993).
[2] *Chemistry and Physics of Solid Surface VII*, edited by R. Vanselow and R. Howe (Springer Verlag, Berlin, 1988).
[3] H.-C. Jeong and E.D. Williams, Surf. Sci. Rep. **34**, 171 (1999).
[4] A. Pimpinelli and J. Villain, *Physics of Crystal Growth* (Cambridge University Press, Cambridge, 1998).
[5] W.K. Burton, N. Cabrela, and F.C. Frank, Philos. Trans. R. Soc. London, Ser. A **243**, 299 (1951).
[6] *Growth and Perfection of Crystals*, edited by R.H. Doremus, B.W. Roberts, and D. Turnbull (Wiley, New York, 1958); A. Ookawa, *Crystal Growth* (Syōkabō, Tokyo, 1977), in Japanese.
[7] Y. Saito, *Statistical Physics of Crystal Growth* (World Scientific, Singapore, 1996).
[8] E.E. Gruber and W.W. Mullins, J. Phys. Chem. Solids **28**, 6549 (1967); V.L. Pokrovsky and A.L. Talapov, Phys. Rev. Lett. **42**, 65 (1979); Sov. Phys. JETP **51**, 134 (1980).
[9] F.D.M. Haldane and J. Villain, J. Phys. (Paris) **42**, 1673 (1981).
[10] T. Izuyama and Y. Akutsu, J. Phys. Soc. Jpn. **51**, 50 (1982); T. Yamamoto and T. Izuyama, *ibid.* **56**, 632 (1987).
[11] C. Jayaprakash, W.F. Saam, and S. Teitel, Phys. Rev. Lett. **50**, 2017 (1983).
[12] H.J. Schultz, J. Phys. (Paris) **46**, 257 (1985); G.F. Gallet, P. Noziéres, S. Balibar, and E. Rolley, Europhys. Lett. **2**, 701 (1986).
[13] H. van Beijeren and I. Nolden, *Structure and Dynamics of Surfaces*, edited by W. Schommers and P. von Blancken-hagen, Vol. 2, p. 259 (Springer-Verlag, Berlin, 1987).
[14] Y. Akutsu, N. Akutsu, and T. Yamamoto, Phys. Rev. Lett. **61**, 424 (1988).
[15] T. Yamamoto, Y. Akutsu, and N. Akutsu, J. Phys. Soc. Jpn. **57**, 453 (1988).
[16] N.C. Bartelt, T.L. Einstein, and E.D. Williams, Surf. Sci. **240**, L591 (1990); B. Joós, T.L. Einstein, and N.C. Bartelt, Phys. Rev. B **43**, 8153 (1991).
[17] S.R. White, Phys. Rev. Lett. **69**, 2863 (1992).
[18] T. Nishino, J. Phys. Soc. Jpn. **64**, 3598 (1995).
[19] T. Nishino and K. Okunishi, J. Phys. Soc. Jpn. **64**, 4084 (1995).
[20] Y. Hieida, K. Okunishi, and Y. Akutsu, Phys. Lett. A **233**, 464 (1997).
[21] K. Okunishi, Y. Hieida, and Y. Akutsu, Phys. Rev. B **59**, 6806 (1999).
[22] K. Okunishi, Y. Hieida, and Y. Akutsu, Phys. Rev. B **60**, R6953 (1999).
[23] N. Akutsu, Y. Akutsu, and T. Yamamoto, Phys. Rev. B **64**, 085415 (2001).
[24] N. Akutsu, Y. Akutsu, and T. Yamamoto, Prog. Theor. Phys. **105**, 361 (2001).
[25] N. Akutsu, Y. Akutsu, and T. Yamamoto, Surf. Sci. **493**, 475 (2001).
[26] K. Sogo, Y. Akutsu, and T. Abe, Prog. Theor. Phys. **70**, 739 (1983); T.T. Truong and M. den Nijs, J. Phys. A **19**, L645 (1986).
[27] M. den Nijs, J. Phys. A **18**, L549 (1985).
[28] B. M. McCoy and T. T. Wu, *The Two-dimensional Ising Model* (Harvard University Press, Cambridge, 1973).
[29] R. J. Baxter, *Exactly Solved Models in Statistical Mechanics* (Academic Press, London, 1982).
[30] A.F. Andreev, Zh. EksP. Theor. Fiz. **80**, 2042 (1981) [Sov. Phys. JETP **53**, 1063 (1982)].
[31] J.B. Kogut, Rev. Mod. Phys. **51**, 659 (1979).
[32] J.J. Métois and J.C. Heyraud, Surf. Sci. **180**, 647 (1987); J.M. Bermond, J.J. Métois, X. Egea, and F. Floret, *ibid.* **330**, 48 (1995); J.M. Bermond, J.J. Métois, J.C. Heyraud, and F. Floret, *ibid.* **416**, 430 (1998).
[33] T. Suzuki, J.J. Métois, and K. Yagi, Surf. Sci. **339**, 105 (1995); T. Suzuki, H. Minoda, Y. Tanishiro, and K. Yagi, Surf. Rev. Lett. **6**, 985 (1999).
[34] K. Arenhold, S. Surnev, H.P. Bonzel, and P. Wynblatt, Surf. Sci. **424**, 271 (1999); S. Surnev, K. Arenhold, P. Coenen, B. Voightländer, k.H.P. Bonzel, and P. Wynblatt, J. Vac. Sci. Technol. A **16**, 1059 (1998).
[35] T. Ohachi and I. Taniguchi, J. Cryst. Growth **65**, 84 (1983); A.V. Babkin, K.O. Keshishev, D.B. Kopeliovich, and A.Ya. Parshin, JETP Lett. **39**, 633 (1984); P.E. Wolf, G.F. Gallet, S. Balibar, E. Rolley, and P. Noziéres, J. Phys. (Paris) **46**, 1987 (1985).
[36] J.E. Avron, J.E. Taylor, and R.K.P. Zia, J. Stat. Phys. **33**, 493 (1983).
[37] C. Rottman and M. Wortis, Phys. Rep. **103**, 59 (1984).
[38] E.D. Williams and N.C. Bartelt, Ultramicroscopy **31**, 36 (1989).
[39] N.C. Bartelt, T.L. Einstein, and C. Rottman, Phys. Rev. Lett. **66**, 961 (1991).
[40] E.D. Williams and N.C. Bartelt, Science **251**, 393 (1991).
[41] H. Hibino and T. Ogino, Phys. Rev. Lett. **72**, 657 (1993); T. Ogino, H. Hibino, and Y. Homma, Crit. Rev. Solid State Mater. Sci. **24**, 227 (1999).
[42] Da-Jiang Liu, J.D. Weeks, M.D. Johnson, and E.D. Williams, Phys. Rev. B **55**, 7653 (1997).
[43] C. Herring, Phys. Rev. **82**, 87 (1951).
[44] C. Rottman and M. Wortis, Phys. Rev. B **24**, 6274 (1981); J.E. Avron, H. van Beijeren, L.S. Schulman, and R.K.P. Zia, J. Phys. A **15**, L81 (1982).
[45] Y. Akutsu and N. Akutsu, J. Phys. A **19**, 2813 (1986).
[46] G. Parisi, *Statistical Field Theory* (Addison-Wesley, Redwood City, California, 1988).

[47] D. J. Amit, *Field Theory, the Renormalization Group, and Critical Phenomena* (McGraw-Hill, New York, 1978).
[48] N. Akutsu and Y. Akutsu, J. Phys. Soc. Jpn. **65**, 1233 (1996).
[49] K. Sudoh, T. Yoshinobu, H. Iwasaki, and E.D. Williams, Phys. Rev. Lett. **80**, 5152 (1998).
[50] V.B. Shenoy, S. Zhang, and W.F. Saam, Phys. Rev. Lett. **81**, 3475 (1998).
[51] M. Horn-von Hoegen, H. Minoda, K. Yagi, F.J. Meyer zu Heringdorf, D. Kähler, and Th. Schmidt, Surf. Sci. **402-404**, 464 (1998); M. Horn-von Hoegen, F.-J. Meyer zu Heringdorf, D. Kähler, Th. Schmidt, and E. Bauer, Thin Solid Films **336**, 16 (1998); H. Minoda, K. Yagi, F.-J. Meyer zu Heringdorf, A. Meier, D. Kähler, and M. Horn-von Hoegen, Phys. Rev. B **59**, 2363 (1999).
[52] H. Minoda and K. Yagi, Phys. Rev. B **60**, 2715 (1999).
[53] J.S. Ozcomert, W.W. Pai, N.C. Bartelt, and J.E. Reutt-Robey, Phys. Rev. Lett. **72**, 258 (1994); J. Vac. Sci. Technol. A **12**, 2224 (1994).
[54] R.A. Marbrow and R.M. Lambert, Surf. Sci. **71**, 107 (1978).
[55] J.B. Maxson, D.E. Savage, F. Liu, R.M. Tromp, M.C. Reuter, and M.G. Lagally, Phys. Rev. Lett. **85**, 2152 (2000).
[56] M. Aono, Y. Fukui, T. Urano, K. Ojima, and M. Yoshimura, Surf. Sci. **507-510**, 417 (2002).
[57] Y. Takahashi, H. Minoda, Y. Tanishiro, and K. Yagi, Surf. Sci. **433-435**, 512 (1999).
[58] S. Fölsch, G. Meyer, K.H. Rieder, M. Horn-von Hoegen, T. Schmidt, and M. Henzler, Surf. Sci. **394**, 60 (1997).
[59] M. Henzler, D. Thielking, M. Horn-von Hoegen, and V. Sielasek, Physica A **261**, 1 (1998).
[60] K. Fujita, Y. Kusumi, and M. Ichikawa, Appl. Phys. Lett. **68**, 631 (1996); Surf. Sci. **357-358**, 490 (1996); Phys. Rev. B **58**, 1126 (1998).
[61] H. Suzuki, H. Nakahara, S. Miyata, and A. Ichimiya, Surf. Sci. **493**, 166 (2001).
[62] A. Natori, Jpn. J. Appl. Phys., Part 1 **33**, 3538 (1994); S. Stoyanov, *ibid.* **30**, 1 (1991); A.V. Latyshev, A.L. Aseev, A.B. Krasilnikov, and S.I. Stenin, Surf. Sci. **213**, 157 (1989); M. Sato, M. Uwaha, and Y. Saito, Phys. Rev. B **62**, 8452 (2000).